Check for updates



Optics Letters

# Characteristics of thin InAlAs digital alloy avalanche photodiodes

WENYANG WANG,[1,2,3,†] JINSHAN YAO,[4,†] JINGYI WANG,[1] ZHUO DENG,[1] ZHIYANG XIE,[1] JIAN HUANG,[1] HONG LU,[4,5,7] AND BAILE CHEN[1,6,8]

[1]School of Information Science and Technology, ShanghaiTech University, Shanghai 201210, China
[2]Shanghai Institute of Microsystem and Information Technology, Chinese Academy of Sciences, Shanghai 200050, China
[3]University of Chinese Academy of Sciences, Beijing 100049, China
[4]National Laboratory of Solid State Microstructures & Department of Materials Science and Engineering, College of Engineering and Applied Sciences, Nanjing University, Nanjing, Jiangsu Province 210093, China
[5]Jiangsu Key Laboratory of Artificial Functional Materials, Nanjing University, Nanjing, Jiangsu Province 210093, China
[6]Shanghai Engineering Research Center of Energy Efficient and Custom AI IC, Shanghai 201210, China
[7]e-mail: hlu@nju.edu.cn
[8]e-mail: chenbl@shanghaitech.edu.cn

Received 23 June 2021; accepted 7 July 2021; posted 8 July 2021 (Doc. ID 435025); published 3 August 2021

**InP-based avalanche photodiodes (APDs) are widely used in short-wave infrared (SWIR) communications. In this work, a thin (200 nm nominal) InAlAs digital alloy layer consisting of two monolayer (ML) InAs and two ML AlAs was grown on InP substrate and investigated in detail. APDs with p-i-n and n-i-p structures were fabricated and characterized. The current-voltage, capacitance-voltage characteristics, and excess noise were measured at room temperature with different laser wavelengths, and the measured effective *k* value (ratio of impact ionization coefficients) is about 0.15 with the multiplication gain up to 12. The randomly-generated path length (RPL) model was carried out to analyze the dead space effect. Our thin digital alloy successfully reduced excess noise compared with conventional $In_{0.52}Al_{0.48}As$ random alloy without introducing new elements and shows the potential for high-speed, low noise APD applications.** © 2021 Optical Society of America

https://doi.org/10.1364/OL.435025

APDs offer higher sensitivity than conventional p-i-n photodiodes due to the internal gain and are widely used in weak optical signals detection [1]. However, the random nature of the impact ionization process produces excess noise, which degrades the signal-to-noise ratio of the detection systems [2]. The excess noise factor F(M) highly depends on the ratio of impact ionization coefficients of holes ($\beta$) and electrons ($\alpha$), based on the classical McIntyre's local field model as below [3]:

$$F(M) = kM + (1 - k)\left(2 - \frac{1}{M}\right), \tag{1}$$

where $k$ is the ratio of the hole ionization coefficient ($\beta$) to that of the electron ($\alpha$). It is clear that excess noise is smaller with lower $k$ values at a given gain $M$. In addition, the gain-bandwidth product is also improved with lower $k$ [4]. It is desirable to use materials with lower $k$ values as the multiplication region in APD structures. InP-based material systems are widely used in SWIR detection due to the availability of multiple lattice matched materials such as InGaAs, InAlAs, InP, and GaAsSb, which offer more degrees of freedom for device design. InP has a large bandgap of 1.42 eV [5] and is often used as a multiplication region in APD design, which can achieve high avalanche gain with a low dark current. However, InP has a $k$ value of 0.4 to 0.5 [6], limiting the signal-to-noise ratio and gain-bandwidth product. $In_{0.52}Al_{0.48}$ As (thereafter InAlAs) is an alternative for the multiplication layer with a lower $k$ ($\sim 0.2$) [7,8]. Recently, periodically grown digital alloys or superlattices showed an even lower excess noise than traditional InAlAs random alloy. $(InAs)_4/(AlAs)_4$ digital alloy with 600 nm thickness has an effective $k$ of about 0.1 [9]. In $(InAs)_3/(AlAs)_3$ digital alloy, the effective $k$ maintained less than 0.01 at multiplication gain up to 6 [10]. In a 6 ML $In_{0.53}Ga_{0.47}$ As/$In_{0.52}Al_{0.48}$ As superlattice, the measured F(M) was lower than the $k = 0$ curve in McIntyre's model at low gain values [11], but excess noise factors at higher gains were not given. Some other materials lattice-matched to InP with low $k$ were also reported recently. $AlAs_{0.56}Sb_{0.44}$ was reported to have an effective $k$ of 0.005, but suffers a high surface leakage current [12]. AlInAsSb random alloy on InP shows a lower dark current compared with AlAsSb and a $k$ value of about 0.018 [13].

The previous works on InAlAs digital alloys were focused on thick devices (600 nm intrinsic layer) and operate at a lower electric field. Generally speaking, a thin multiplication region should be employed to achieve a large gain-bandwidth product for high speed operation because of shorter transit time. The noise performance of the thin InAlAs digital alloys has not been studied so far, to the best of our knowledge. In this work, we investigated the p-i-n and n-i-p APDs with a 200 nm (nominal) InAlAs digital alloy intrinsic layer, which could be potentially used in high-speed APD structures. The digital alloys in this work have a period of four monolayers, and each period contains

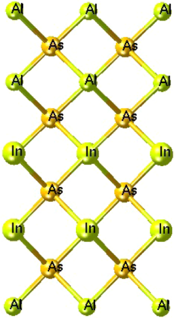


**Fig. 1.** Supercell of our digital alloy showing the growth order of InAs and AlAs layers.

two ML InAs and two ML AlAs. Current-voltage (I-V) characteristics and capacitance-voltage (C-V) characteristics were measured, and impact ionization coefficients of electrons and holes in our digital alloy were calculated. Moreover, the dead space effect in our digital alloy APDs was also analyzed. The excess noise measurements with 532, 594, and 633 nm lasers for p-i-n and n-i-p structures were carried out. The measured effective *k* in pure electron injection p-i-n structure is about 0.15 with multiplication gain below 12. Another p-i-n sample with $In_{0.52}Al_{0.48}As$ random alloy intrinsic layer was also measured for comparison.

The APD structures were grown on semi-insulating InP substrates by molecular beam epitaxy (MBE) as shown in Fig. 1(a) and Fig. 1(b). The p-i-n wafers contain a 100 nm lattice-matched $In_{0.53}Ga_{0.47}As$ (thereafter InGaAs) heavily p-doped (Be, $10^{19}$ $cm^{-3}$) contact layer on the top, a 300 nm p-doped ($10^{18}$ $cm^{-3}$) InAlAs top cladding layer, an 200 nm thick undoped InAlAs digital or random layer (samples A and C), a 100 nm n-doped (Si, $10^{18}$ $cm^{-3}$) InAlAs bottom cladding layer, and a 500 nm heavily n-doped ($5 \times 10^{18}$ $cm^{-3}$) InAlAs contact layer at the bottom. The n-i-p digital alloy APD wafer (sample B) is very similar to the p-i-n wafer (sample A) except that the doping sequence is reverted, and the details of the samples are given in Table 1. The mesas were processed using a solution of $H_2SO_4 : H_2O_2 : H_2O$ (1: 8: 80) and passivated by silicon nitride thin film grown by ICPCVD. The contacts were made of 20 nm Ti, 30 nm Pt, and 100 nm Au and deposited with electron beam evaporator. A 360°C rapid thermal annealing was performed to ensure good ohmic contacts. Capacitance-voltage (C-V) characteristics of the 100-μm-diameter devices were measured at room temperature, and the thicknesses of the intrinsic layers were estimated.

Current-voltage (I-V) characteristics were measured at room temperature (Figs. 2 and 3) to calculate the multiplication gains. Lasers were focused at the center on the top of the mesa to maximize the absorption in the top cladding layer

**Table 1. Details of the Samples Used in This Work**

| Sample | Structure | Intrinsic Layer Material | Intrinsic Layer Thickness (Nominal/Fitted, nm) |
|---|---|---|---|
| A | p-i-n | $(InAs)_2/(AlAs)_2$ | 200/225 |
| B | n-i-p | $(InAs)_2/(AlAs)_2$ | 200/220 |
| C | p-i-n | $In_{0.52}Al_{0.48}As$ | 200/125 |

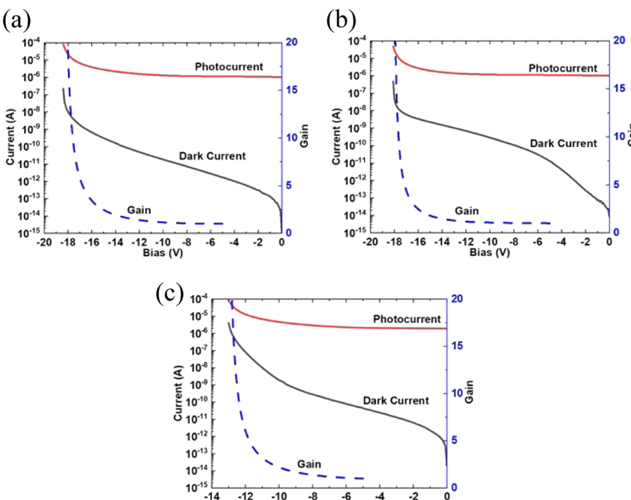


**Fig. 2.** Photocurrent, dark current and multiplication gain of (a) digital alloy p-i-n, (b) digital alloy n-i-p, and (c) random alloy p-i-n APDs, measured with 532 nm laser at room temperature.

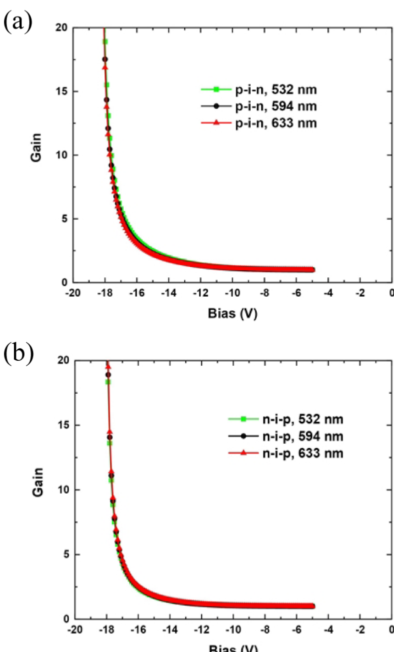


**Fig. 3.** Measured gain versus bias voltage of (a) digital alloy p-i-n and (b) digital alloy n-i-p APDs with 532, 594, and 633 nm lasers.

and prevent illumination on the sidewall. The breakdown voltages of samples A, B, and C are −18.5 V, −18.2 V, and −13.1 V, respectively. The corresponding dark current densities at 90% breakdown voltage are 14.4, 52.3, and 535 $\mu A/cm^2$, respectively.

The multiplication gain is defined as the ratio of multiplied photocurrent to the photocurrent at unit gain. The unit gain point was set at −5 V and photocurrents were flat at low bias voltages. The gain calculations for all the samples have considered the increase of injected photocurrent with reverse bias due to the widening of the depletion width [12,14]. The 532 nm laser was absorbed more strongly than the 594 and 633 nm lasers in the contact layer and top cladding layer [15,16], which

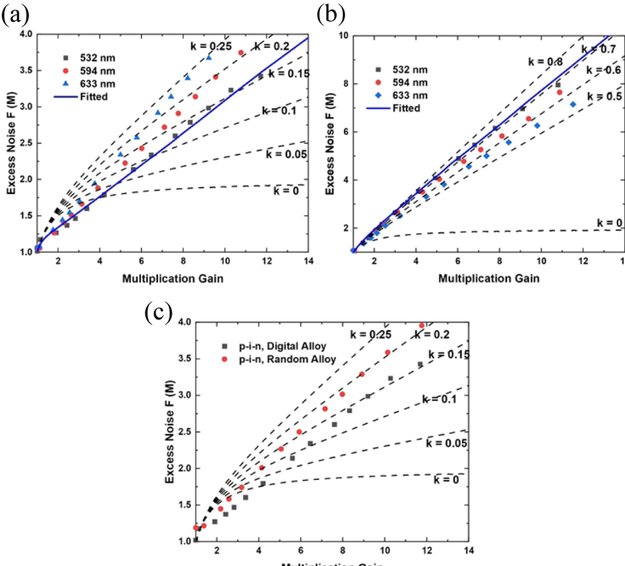


**Fig. 4.** Excess noise factor versus gain of (a) digital alloy p-i-n and (b) digital alloy n-i-p APDs, respectively, with 532, 594, and 633 nm lasers. The local field model curves are presented for comparison. Fitted curves from RPL model are also present. The excess noise measured with 532 nm laser for (c) comparison of digital alloy p-i-n and random alloy p-i-n.

produces pure electron and hole injection profiles in p-i-n and n-i-p samples, respectively. It is noted in Fig. 4 that the laser with a shorter wavelength produces a larger multiplication in p-i-n sample A but a smaller one in the n-i-p sample B, indicating that the impact ionization coefficient of electrons ($\alpha$) is greater than holes ($\beta$) [17], which is also consistent with the results of excess noise characterizations as shown in Fig. 4.

The excess noise factors were measured using a noise figure meter. As shown in Fig. 4(a), the measured F(M) in digital alloy p-i-n APD with 532 nm laser illumination is lower than the other wavelengths, and the effective $k$ stayed about 0.15 with the multiplication gain up to 12, which is lower than that of the random alloy p-i-n APD ($k \approx 0.2$) as shown in Fig. 4(c). In the n-i-p APD, the effective $k$ value increases as the wavelength decreases as expected. In the local field model, the measured effective $k$ value with pure holes injection should be the reciprocal of that with pure electron injection. However, under the illumination of a 532 nm laser, the measured $k$ value in n-i-p is only between 0.7 and 0.8, which is much smaller than the reciprocal of effective $k$ in the digital alloy p-i-n. Moreover, the measured excess noise factors at low-gain region in p-i-n samples are lower than any curve in McIntyre's local field model, which indicates that the dead space effect in these APDs may be significant and should be included in the impact ionization coefficients analysis.

Carriers need to travel in the electric field to accumulate enough energy to initiate an impact ionization, and the minimum distance needed to travel is defined as "dead space." In thin multiplication layers, when the dead space is comparable with the thickness of the multiplication layer, the randomness of positions of impact ionizations is reduced, and so does the excess noise [18–20]. A simplified randomly-generated ionization path length (RPL) nonlocal model with Monte Carlo framework was adopted to analyze the impact ionization coefficients and dead space effect. Here, the path lengths of electrons ($l_e$) and holes ($l_h$) before an impact ionization are:

$$l_e = \frac{E_{th,e}}{q\varepsilon} - \frac{\ln(r)}{\alpha^*}, \tag{2}$$

$$l_h = \frac{E_{th,h}}{q\varepsilon} - \frac{\ln(r')}{\beta^*}, \tag{3}$$

where $E_{th,e}$ and $E_{th,h}$ are effective threshold energies for electrons and holes to impact ionize, $\varepsilon$ is the electric field intensity, $\alpha^*$ and $\beta^*$ are the effective impact ionization coefficients after the dead space, $r$ and $r'$ are randomly independently generated numbers uniformly distributed between 0 and 1. The details of the calculations are given in reference [21]. As shown in Figs. 4 and 5, both gain and excess noise factor are fitted well to experimental results with 532 nm laser illumination.

The fitted effective impact ionization coefficients after the dead space of the digital alloy are:

$$\alpha^* = 1.1 \times 10^6 \times \exp\left(-\left(\frac{1.01 \times 10^6}{\varepsilon}\right)^{1.95}\right), \tag{4}$$

$$\beta^* = 4.8 \times 10^5 \times \exp\left(-\left(\frac{1.02 \times 10^6}{\varepsilon}\right)^{2.2}\right), \tag{5}$$

and the fitted effective threshold energies are $E_{th,e} = 3.5$ eV and $E_{th,h} = 3.5$ eV. These threshold values are higher than that in previous Monte-Carlo simulation [22], which is due to the fact that scattering mechanisms are not considered in the RPL model.

The effective $k$ values of both p-i-n and n-i-p decreased with the dead space effect included, which explains the fact that p-i-n

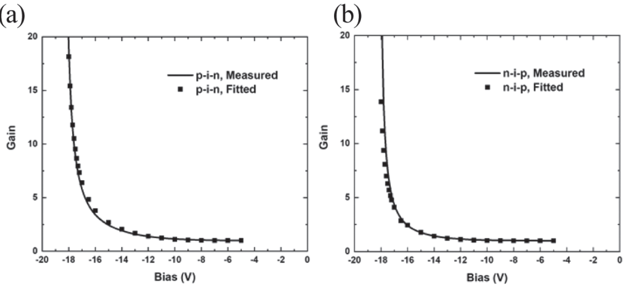


**Fig. 5.** Fitted and measured (532 nm laser) multiplication gain versus bias voltage for (a) digital alloy p-i-n and (b) digital alloy n-i-p APDs.

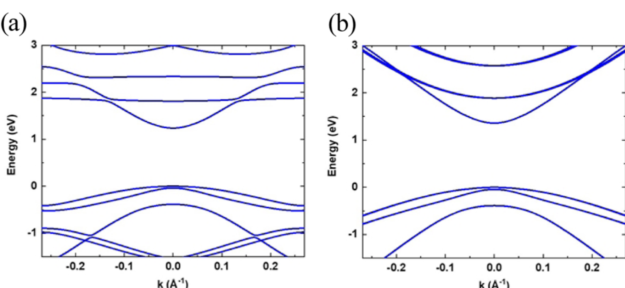


**Fig. 6.** $E - k$ relationship of the (a) InAlAs digital alloy and (b) random alloy along the growth direction [1].

and n-i-p structures do not yield an effective value of $k_{eff}$ and $1/k_{eff}$. On the other hand, the fitted impact ionization coefficients show that the value of $\beta/\alpha$ increases with the electric field, which is similar to that of InAlAs random alloy [7,23]. In thin p-i-n APDs, higher electric fields are required to achieve the same gain as the thicker ones. As the electric field increases, the impact ionization ratio of electron and hole tends to be unity, which could increase the excess noise. The $E-k$ relationships along the growth direction [001] were calculated using the Venna *ab initio* simulation package (VASP) [24,25] and screened hybrid functional of Heyd, Scuseria, and Ernzerhof (HSE06) [26,27], as shown in Fig. 6. The calculated effective masses for electron and hole in conduction band and valence band along the growth direction [1] in digital alloy are 0.071 and 0.358 $m_0$, respectively, while in the random alloy, these values are 0.072 for electrons and 0.22 $m_0$ for holes. The difference of effective masses is larger in the digital alloy, producing more dissimilar impact ionization coefficients and smaller excess noise. Unlike the digital alloys with more monolayers, our digital alloy does not produce a minigap near the top of the valance band, and holes are not impeded from gaining energy when traveling along the electric field. That could be why the excess noise of the InAlAs digital alloy in this work is slightly higher than the previously reported values [9,10]. However, digital alloy with a longer period has a smaller bandgap [28], which may correspond to a higher tunneling current and may limit the ability to operate under a high electric field.

In conclusion, APDs with a thin short-period $(InAs)_2/(AlAs)_2$ digital alloy layer were fabricated and characterized. Our digital alloy showed lower excess noise compared with $In_{0.52}Al_{0.48}$ As random alloy. Both p-i-n and n-i-p devices were measured to analyze the impact ionization coefficients and the influence from the dead space effect. The low excess noise and low dark current in thin APDs with high electric field show the potential in high-speed separate absorption, grading, charge, and multiplication (SAGCM) APD applications, and the digital alloy can be a good alternative for InAlAs random alloy as the multiplication layer.

**Funding.** National Key Research and Development Program of China (2018YFB2201000); National Natural Science Foundation of China (61975121).

**Disclosures.** The authors declare no conflicts of interest.

**Data Availability.** Data underlying the results presented in this paper are not publicly available at this time but may be obtained from the authors upon reasonable request.

†These authors contributed equally to this Letter.

## REFERENCES

1. J. C. Campbell, J. Lightwave Technol. **34**, 278 (2016).
2. B. Chen, Y. Wan, Z. Xie, J. Huang, N. Zhang, C. Shang, J. Norman, Q. Li, Y. Tong, and K. M. Lau, ACS Photon. **7**, 528 (2020).
3. R. J. McIntyre, IEEE Trans. Electron Devices ED-**13**, 164 (1966).
4. R. B. Emmons, J. Appl. Phys. **38**, 3705 (1967).
5. I. Vurgaftman, J. R. Meyer, and L. R. Ram-Mohan, J. Appl. Phys. **89**, 5815 (2001).
6. C. A. Armiento and S. H. Groves, Appl. Phys. Lett. **43**, 198 (1983).
7. Y. L. Goh, A. R. J. Marshall, D. J. Massey, J. S. Ng, C. H. Tan, M. Hopkinson, J. P. R. David, S. K. Jones, C. C. Button, and S. M. Pinches, IEEE J. Quantum Electron. **43**, 503 (2007).
8. C. Lenox, P. Yuan, H. Nie, O. Baklenov, C. Hansing, J. C. Campbell, A. L. Holmes, Jr., and B. G. Streetman, Appl. Phys. Lett. **73**, 783 (1998).
9. Y. Yuan, J. Zheng, Y. Tan, Y. Peng, A.-K. Rockwell, S. R. Bank, A. Ghosh, and J. C. Campbell, Photon. Res. **6**, 794 (2018).
10. J. Zheng, Y. Yuan, Y. Tan, Y. Peng, A. K. Rockwell, S. R. Bank, A. W. Ghosh, and J. C. Campbell, J. Lightwave Technol. **36**, 3580 (2018).
11. S. Lee, M. Winslow, C. H. Grein, S. H. Kodati, A. H. Jones, D. R. Fink, P. Das, M. M. Hayat, T. J. Ronningen, J. C. Campbell, and S. Krishna, Sci. Rep. **10**, 16735 (2020).
12. X. Yi, S. Xie, B. Liang, L. W. Lim, J. S. Cheong, M. C. Debnath, D. L. Huffaker, C. H. Tan, and J. P. R. David, Nat. Photonics **13**, 683 (2019).
13. S. H. Kodati, S. Lee, B. Guo, A. H. Jones, M. Schwartz, M. Winslow, N. A. Pfiester, C. H. Grein, T. J. Ronningen, J. C. Campbell, and S. Krishna, Appl. Phys. Lett. **118**, 091101 (2021).
14. M. H. Woods, W. C. Johnson, and M. A. Lampert, Solid-State Electron. **16**, 381 (1973).
15. M. Lumb, M. Yakes, M. Gonzalez, and J. Tischler, J. Appl. Phys. **114**, 103504 (2013).
16. M. N. Muñoz, T. M. Holden, F. H. Pollak, M. Kahn, D. Ritter, L. Kronik, and G. M. Cohen, J. Appl. Phys. **92**, 5878 (2002).
17. Y. Yuan, J. Zheng, A. K. Rockwell, S. D. March, S. R. Bank, and J. C. Campbell, IEEE Photon. Technol. Lett. **31**, 315 (2019).
18. M. M. Hayat, B. E. A. Saleh, and M. C. Teich, IEEE Trans. Electron Devices **39**, 546 (1992).
19. M. A. Saleh, M. M. Hayat, B. E. A. Saleh, and M. C. Teich, IEEE Trans. Electron Devices **47**, 625 (2000).
20. E. Jamil, J. S. Cheong, J. P. R. David, and M. M. Hayat, Opt. Express **24**, 21597 (2016).
21. D. S. Ong, K. F. Li, G. J. Rees, J. P. R. David, and P. N. Robson, J. Appl. Phys. **83**, 3426 (1998).
22. J. Zheng, Y. Yuan, Y. Tan, Y. Peng, A. Rockwell, S. R. Bank, A. W. Ghosh, and J. C. Campbell, Appl. Phys. Lett. **115**, 171106 (2019).
23. Y. L. Goh, D. J. Massey, A. R. J. Marshall, J. S. Ng, C. H. Tan, W. K. Ng, G. J. Rees, M. Hopkinson, J. P. R. David, and S. K. Jones, IEEE Trans. Electron Devices **54**, 11 (2007).
24. G. Kresse and J. Furthmüller, Comput. Mater. Sci. **6**, 15 (1996).
25. G. Kresse and J. Furthmüller, Phys. Rev. B **54**, 11169 (1996).
26. J. Heyd, G. E. Scuseria, and M. Ernzerhof, J. Chem. Phys. **124**, 219906 (2006).
27. J. Heyd, G. E. Scuseria, and M. Ernzerhof, J. Chem. Phys. **118**, 8207 (2003).
28. J. Zheng, Y. Tan, Y. Yuan, A. W. Ghosh, and J. C. Campbell, J. Appl. Phys. **125**, 245702 (2019).